IEEE Access
Multidisciplinary ⋮ Rapid Review ⋮ Open Access Journal

Received October 9, 2020, accepted October 20, 2020, date of publication October 26, 2020, date of current version November 9, 2020.

Digital Object Identifier 10.1109/ACCESS.2020.3033889

Research on the Harmonics Penetration Characteristics of the Traction Network to Three-Phase 380 V Power System of the Traction Substation and Suppression Scheme

YUANZHE ZHAO[1,2,3,4], (Member, IEEE), LINJIE REN[1,2,3,4], (Graduate Student Member, IEEE), GUOBIN LIN[4], AND FEI PENG[5], (Member, IEEE)

[1]College of Transportation Engineering, Tongji University, Shanghai 201804, China
[2]Ministry of Education, Key Laboratory of Road and Traffic Engineering, Shanghai 201804, China
[3]Key Laboratory of Rail Infrastructure Durability and System Safety, Tongji University, Shanghai 201804, China
[4]National Maglev Transportation Engineering Research and Development Center, Tongji University, Shanghai 201804, China
[5]College of Electrical Engineering, Qingdao University, Qingdao 266071, China

Corresponding author: Guobin Lin (linguobin@tongji.edu.cn)

This work was supported in part by the National Key Technology Research and Development Program of China under Grant 2016YFB1200602, and in part by the Project of Science and Technology Commission Shanghai Municipality under Grant 17511102302.

ABSTRACT To reveal the penetration characteristics of high-frequency harmonics of the traction network to the three-phase 380 V power system in the traction substation (TSS), the harmonic equivalent circuit model and harmonic penetration mathematical model of the two-phase to three-phase Scott-T transformer are established. Through the power quality measurement and harmonic analysis, the results indicate that the high-frequency harmonics in the traction network will severely penetrate the three-phase 380 V power system, which will cause almost the same degree of harmonic distortion, verifying the correctness of the harmonic penetration model. To filter high-frequency harmonics in TSS, a novel structure of high-pass filter (HPF) is proposed that features with high-pass characteristic at high frequencies while high-impedance at fundamental frequency. Furthermore, a set of three-phase experimental device is developed, and a long-term filtering experiment in the TSS is performed. The experimental results show that the novel HPF experimental device can effectively filter out high-frequency harmonics of the three-phase 380 V power system, and have almost no loss and reactive power. The feasibility and effectiveness of the suppression scheme based on the novel HPF are verified.

INDEX TERMS High-frequency harmonic, Scott-T transformer, harmonic penetration, high-pass filter.

I. INTRODUCTION

In recentyears, electrified railways, especially heavy-haul and high-speed railways, have been rapidly developing in China. In this field, increasingly more AC-DC-AC electric trains are widely used owing to the advantages of the heavier traction load, the higher power factor and less low-order harmonic contents [1]–[3]. Due to the application of pulse-width modulation four-quadrant converters, a certain number of high-frequency harmonic currents near the converter switching frequency are generated by ac-dc-ac trains [4]. If the frequency of harmonic currents injected into the traction network matches the natural resonance frequency of the traction power supply system (TPSS), high-frequency harmonic resonance will occur. The resonance phenomenon can cause excessively high harmonic voltages and currents, severe voltage distortion and overvoltage [5], which can endanger the safe operation of trains and traction power supply equipment. As serious power quality problem in electrified railways, the resonance phenomenon has appeared in many countries, such as Switzerland, Italy, South Korea, and China [6]–[9].

Research on the resonance of electrified railways mainly focuses on the occurrence mechanism and influencing factors, where the primary methods are online

The associate editor coordinating the review of this manuscript and approving it for publication was Zhigang Liu.

measurement [10], [11], simulation model analysis [9], [12], [13] and mathematical analysis [14]–[16]. Reference [10] proposes an online identification method, and [11] uses a butterfly-type disturbance circuit and a chirped-pulse-width-modulated signal model to propose a controlled wide-bandwidth impedance measurement. Based on the multi-transmission line theory [12], [9], and [13] established a detailed simulation model of the TPSS, and impedance frequency characteristics and harmonic amplification features are analyzed under various conditions. References [14] and [15] present the resonance mode analysis and modal sensitivity analysis by using the nodal admittance matrix of the TPSS and the train. In addition, [16] analyzes the harmonic stability by establishing the small-signal state-space model of the train-network system and utilizing the eigenvalue-based method.

Through the analysis of different approaches, detailed information about the resonance mechanism and influencing factors can be obtained, which has guiding significance for the early design of the TPSS and resonance suppression scheme.

However, all of these studies are limited to the traction network side (27.5 kV) and public power grid side (110 kV or 220 kV), and do not consider the effect of high-frequency harmonics on the three-phase 380 V power supply system in the traction substation (TSS). In some electrified railway lines with high content of high-frequency harmonics, problems, such as reduced service life, and burnout of electrical equipment in the TSS, have frequently occurred. Therefore, it is necessary to study the penetration characteristics of high-frequency harmonics into the three-phase 380 V power system and propose an effective harmonic suppression scheme to ensure the safety of electrical equipment in the TSS, which is often overlooked in previous studies.

At present, the studies of traction network resonance and high-frequency harmonic suppression are focus on two methods. One method is to improve trains to suppress characteristic harmonics, which mainly includes installing a filtering device [17], optimizing the control strategy of the main converters to eliminate the characteristic harmonics [18]–[20], and harmonic compensation using auxiliary converters [21]. However, due to the type variety, internal structure limitations of trains, and the different resonance frequencies of different power supply intervals, the resonance suppression of the entire line is challenging to realize from the train perspective.

The other method is to install passive high-pass filter (HPF) in the TSS or sectioning post, such as first-, second-, third-order and C-type, which is a simple, reliable, and easy-to-implement approach to effectively filter out high-frequency harmonics and address resonance issues [22]–[24]. Nevertheless, one- and two-order HPFs have large fundamental losses due to the series resistor of the filter branch, especially first-order HPF [22]. The third-order HPF exhibits very small fundamental loss, but it will introduce an additional parallel resonance point below the original resonance point. The C-type HPF described in [23], [24] shows better comprehensive performance and almost has no fundamental loss, but it is sensitive to parameter variation.

These HPFs are capacitive at the fundamental frequency. Due to the widespread application of AC-DC-AC trains, the system has very little demand for capacitive reactive power. The capacitive reactive power generated by these HPFs can overcompensate for the system, affect the system power factor and increase the traction network voltage.

In [25], [26], a hybrid passive filter is proposed, which can filter out high-order harmonics without generating reactive power. However, this filter requires a series capacitor and inductor in the system, which is not suitable for the TPSS. A novel type of wave-trap HPF (NHPF) proposed in [27], [28] can filter out high-frequency harmonics and exhibit extremely high impedance at the fundamental frequency, which implies no fundamental loss or reactive power. However, the performance of this type of HPF has not been verified by experimental analysis. Therefore, further research on this novel type of HPF need be conducted.

In some electrified railway lines, high-frequency harmonics have not caused harmful effects to electrical equipment and trains on the traction network side. Therefore, the installation of the filter on the 380 V power system side could be given priority to eliminate the harm of high-frequency harmonics.

The contributions of this paper are as follows.

1) Through the establishment of the harmonic penetration model of a two-phase to three-phase step-down Scott-T transformer and the analysis of measured data, the effect of high-frequency harmonics of the traction network on the three-phase 380 V power system in TSS is studied for the first time, which is a necessary supplement to the transmission characteristics research of high-frequency harmonics in the TPSS.
2) A harmonic suppression scheme based on NHPF for the three-phase 380 V power system of the TSS is proposed. In addition, a set of experimental devices developed has solved the high-frequency harmonics problems in TSS, the characteristics of high-pass at high frequencies and high-impedance at the fundamental frequency of NHPF are verified.

The rest of this paper is organized as follows. In section II, the harmonic equivalent circuit and harmonic penetration mathematical model of two-phase to three-phase Scott-T transformer are established. Section III presents a novel structure of HPF and introduces its filtering principle. A harmonic suppression scheme for the three-phase system is proposed. In section IV, the power quality of the TSS with high harmonic contents is measured, and the characteristic harmonic distribution of the traction network and the penetration characteristic of the harmonics into the three-phase 380 V system are analyzed. In section V, a set of three-phase HPF experimental devices is developed and installed in the measured TSS to verify its filtering effect. The conclusion of this paper is summarized in section VI.

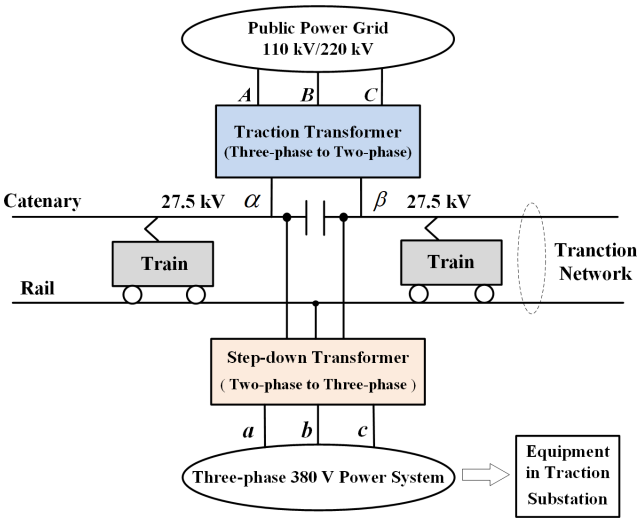

FIGURE 1. The traction power supply system with three-phase 380 V power system.

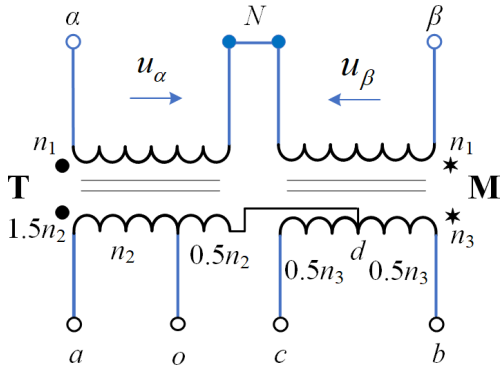

FIGURE 2. The structure of the Scott-T transformer.

II. HARMONIC PERMEABILITY MODEL OF TWO-PHASE TO THREE-PHASE SCOTT-T TRANSFORMER

A. THREE-PHASE 380 V POWER SYSTEM IN TSS

The electrical equipment in the TSS, such as the battery system, the relay protection system, computer, and lighting, are supplied power by the three-phase 380 V power system. There are two methods to obtained three-phase 380 V power system. One method is to employ the three-phase 10kV of the public power grid; the other method is to use step-down transformer, which can transform the two single-phase 27.5 kV of the traction network into three-phase 380 V, as shown in Fig. 1. The two methods are mutually reserved.

B. HRAMONIC PERMEABILITY MODEL BEASED ON SCOTT-T TRANSFORMER

Generally, the phase difference between two single-phase voltages of the traction network is 60° or 90°. When it is 90°, the Scott-T transformer can be utilized as the step-down transformer to convert the two single-phase 27.5 kV voltages into three-phase symmetrical voltages for the electrical equipment in the TSS. Fig. 2 shows the specific structure of the Scott-T transformer to achieve this conversion [29].

In Fig. 2, the Scott-T transformer contains two single-phase transformers: the main transformer (M) and teaser transformer (T). The primary winding of the main transformer is connected to the β-phase of the traction network, while the secondary winding is connected to line-b and line-c, and center-tapped at d. Moreover, the primary winding of the teaser transformer is connected to the α-phase of the traction network, and the secondary winding is connected to line-a and the tapping d of the main transformer. Tap-o at two thirds of the secondary winding is the neutral point of the three-phase system. Furthermore, line-a, line-b, line-c and neural line-o on the secondary side form a three-phase four-wire system.

The number of turns of the primary winding for the main transformer and teaser transformer is n_1; the number of turns of the secondary winding of the main transformer is $1.5n_2$; the numbers of turns in portion ao and od are n_2 and $0.5n_2$, respectively; the number of turns of the secondary winding of the main transformer is n_3; d divides the secondary winding bc into two halves. The relationship between n_2 and n_3 is $n_3/n_2 = \sqrt{3}$.

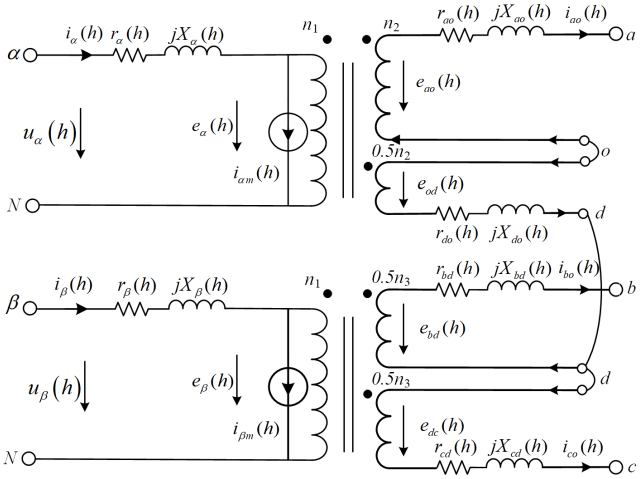

FIGURE 3. Harmonic equivalent circuit model of Scott-T transformer.

According to the structure and position of the winding tap of the Scott-T transformer, the harmonic equivalent circuit model is established, as shown in Fig. 3. The secondary windings of M are equivalent to two windings ao and od, and the secondary windings of T are equivalent to two windings of bd and dc. When the harmonic penetration model is established, the saturation of the self-leakage inductance and mutual leakage inductance is ignored.

Fig. 3 shows the harmonic penetration model under the h-order harmonic, where h is the harmonic order that is the ratio of the harmonic frequency to the fundamental frequency. On the primary side, $u_\alpha(h)$ and $u_\beta(h)$ are the h-order harmonic voltages of the α-phase and β-phase caused by the traction network currents and background harmonic in the traction network; $i_\alpha(h)$ and $i_\beta(h)$ are the input harmonic currents of the α-phase and β-phase; $e_\alpha(h)$ and $e_\beta(h)$ are the harmonic

excitation voltages of the α-phase and β-phase windings; $i_{\alpha m}(h)$ and $i_{\beta m}(h)$ are the harmonic excitation currents of α-phase and β-phase windings. On the secondary side, $i_{ao}(h)$, $i_{bo}(h)$ and $i_{co}(h)$ are harmonic currents between each phase line and the neutral line; $e_{ao}(h)$, $e_{od}(h)$, $e_{bd}(h)$ and $e_{dc}(h)$ are the harmonic excitation voltages of each winding. $r_\alpha(h)$, $r_\beta(h)$, $r_{ao}(h)$, $r_{od}(h)$, $r_{bd}(h)$ and $r_{dc}(h)$ denote the harmonic resistances of the corresponding windings; $X_\alpha(h), X_\beta(h)$, $X_{ao}(h)$, $X_{od}(h)$, $X_{bd}(h)$ and $X_{dc}(h)$ are the harmonic leakage resistances of the corresponding windings. The relationship between harmonic impedance and fundamental impedance is $z(h) = r\,(h) + jX\,(h) = \sqrt{h}r\,(1) + jhX\,(1)$.

Then, the leakage impedance of the primary and secondary windings can be expressed as:

$$\begin{cases} z_\alpha(h) = r_\alpha(h) + jX_\alpha(h) \\ z_\beta(h) = r_\beta(h) + jX_\beta(h) \end{cases} \tag{1}$$

$$\begin{cases} z_{ao}(h) = r_{ao}(h) + jX_{ao}(h) \\ z_{bd}(h) = r_{bd}(h) + jX_{bd}(h) \\ z_{cd}(h) = r_{cd}(h) + jX_{cd}(h) \\ z_{od}(h) = r_{od}(h) + jX_{od}(h) \end{cases} \tag{2}$$

where $z_\alpha(h)$, $z_\beta(h)$, $z_{ao}(h)$, $z_{od}(h)$, $z_{bd}(h)$ and $z_{dc}(h)$ denote the equivalent leakage impedances of the corresponding windings.

According to the circuit of the secondary side in Fig. 3, the three-phase harmonic voltages are acquired as follows.

$$\begin{cases} u_{ao}(h) = e_{ao}\,(h) - i_{ao}(h)z_{ao}(h) \\ u_{bo}(h) = e_{bd}\,(h) - e_{od}\,(h) - i_{bo}(h)(z_{bd}(h) + z_{od}(h)) \\ \qquad\quad - i_{co}(h)z_{od}(h) \\ u_{co}(h) = -e_{dc}\,(h) - e_{od}\,(h) - i_{co}(h)(z_{cd}(h) + z_{od}(h)) \\ \qquad\quad - i_{bo}(h)z_{od}(h) \end{cases} \tag{3}$$

where $u_{ao}(h)$, $u_{bo}(h)$ and $u_{co}(h)$ are the harmonic voltages of the corresponding ports on the secondary side.

The relationship between the excitation voltages of the four secondary windings and those of the two primary windings is

$$\begin{bmatrix} e_{ao}\,(h) \\ e_{od}\,(h) \\ e_{bd}\,(h) \\ e_{dc}\,(h) \end{bmatrix} = \begin{bmatrix} n_2/n_1 & 0 \\ n_2/2n_1 & 0 \\ 0 & n_3/2n_1 \\ 0 & n_3/2n_1 \end{bmatrix} \begin{bmatrix} e_\alpha\,(h) \\ e_\beta\,(h) \end{bmatrix}. \tag{4}$$

The electrical equation of the primary circuit is as follows

$$\begin{cases} e_\alpha(h) = i_{\alpha m}\,(h)\,z_{\alpha m}(h) = u_\alpha(h) - i_\alpha\,(h)\,z_\alpha(h) \\ e_\beta(h) = i_{\beta m}\,(h)\,z_{\beta m}(h) = u_\beta(h) - i_\beta\,(h)\,z_\beta(h) \\ i_\alpha\,(h) = \dfrac{n_2}{n_1} i_{ao}\,(h) - \dfrac{n_2}{2n_1}\,(i_{bo}\,(h) + i_{co}\,(h)) + i_{\alpha m}\,(h) \\ i_\beta\,(h) = \dfrac{n_3}{2n_1}\,(i_{bo}\,(h) - i_{co}\,(h)) + i_{\beta m}\,(h) \end{cases} \tag{5}$$

where, $z_{\alpha m}(h) = jX_{\alpha m}(h)$ and $z_{\beta m}(h) = jX_{\beta m}(h)$ are the excitation impedances of the α-phase and β-phase windings, respectively.

The harmonic excitation voltages $e_\alpha(h)$ and $e_\beta(h)$ can be derived by (5), which are expressed as

$$\begin{cases} e_\alpha(h) = \dfrac{u_\alpha(h)}{1 + z_\alpha(h)/z_{\alpha m}(h)} \\ \qquad\quad - \dfrac{\frac{n_2}{2n_1}\,(2i_{ao}\,(h) - i_{bo}\,(h) - i_{co}\,(h))\,z_\alpha(h)}{1 + z_\alpha(h)/z_{\alpha m}(h)} \\ e_\beta(h) == \dfrac{u_\beta(h)}{1 + z_\beta(h)/z_{\beta m}(h)} - \dfrac{\frac{n_3}{2n_1}\,(i_{bo}\,(h) - i_{co}(h))\,z_\beta(h)}{1 + z_\beta(h)/z_{\beta m}(h)} \end{cases} \tag{6}$$

Substituting (4) and (6) into (3) yields:

$$\begin{cases} u_{ao}(h) = \dfrac{\frac{n_2}{n_1}u_\alpha(h)}{1 + z_\alpha(h)/z_{\alpha m}(h)} \\ \qquad\quad - \dfrac{\frac{n_2^2}{2n_1^2}\,(2i_{ao}\,(h) - i_{bo}\,(h) - i_{co}\,(h))\,z_\alpha(h)}{1 + z_\alpha(h)/z_{\alpha m}(h)} \\ \qquad\quad - i_{ao}\,(h)\,z_{ao}(h) \\ u_{bo}(h) = \dfrac{\frac{n_3}{2n_1}u_\beta(h)}{1 + z_\beta(h)/z_{\beta m}(h)} - \dfrac{\frac{n_3^2}{4n_1^2}\,(i_{bo}\,(h) - i_{co}\,(h))\,z_\beta(h)}{1 + z_\beta(h)/z_{\beta m}(h)} \\ \qquad\quad - \dfrac{\frac{n_2}{2n_1}u_\alpha(h)}{1 + z_\alpha(h)/z_{\alpha m}(h)} \\ \qquad\quad + \dfrac{\frac{n_2^2}{4n_1^2}\,(2i_{ao}\,(h) - i_{bo}\,(h) - i_{co}\,(h))\,z_\alpha(h)}{1 + z_\alpha(h)/z_{\alpha m}(h)} \\ \qquad\quad - i_{bo}(h)(z_{bd}(h) + z_{od}(h)) - i_{co}(h)z_{od}(h) \\ u_{co}(h) = -\dfrac{\frac{n_3}{2n_1}u_\beta(h)}{1 + z_\beta(h)/z_{\beta m}(h)} + \dfrac{\frac{n_3^2}{4n_1^2}\,(i_{bo}\,(h) - i_{co}\,(h))\,z_\beta(h)}{1 + z_\beta(h)/z_{\beta m}(h)} \\ \qquad\quad - \dfrac{\frac{n_2}{2n_1}u_\alpha(h)}{1 + z_\alpha(h)/z_{\alpha m}(h)} \\ \qquad\quad + \dfrac{\frac{n_2^2}{4n_1^2}\,(2i_{ao}\,(h) - i_{bo}\,(h) - i_{co}\,(h))\,z_\alpha(h)}{1 + z_\alpha(h)/z_{\alpha m}(h)} \\ \qquad\quad - i_{co}(h)(z_{dc}(h) + z_{od}(h)) - i_{bo}(h)z_{od}(h) \end{cases} \tag{7}$$

When the secondary side is unloaded, the three-phase harmonic currents are zero; then, (7) is simplified as

$$\begin{cases} u_{ao}(h) = \dfrac{\frac{n_2}{n_1}u_\alpha(h)}{1 + z_\alpha(h)/z_{\alpha m}(h)} \\ u_{bo}(h) = \dfrac{\frac{n_3}{2n_1}u_\beta(h)}{1 + z_\beta(h)/z_{\beta m}(h)} - \dfrac{\frac{n_2}{2n_1}u_\alpha(h)}{1 + z_\alpha(h)/z_{\alpha m}(h)} \\ u_{co}(h) = -\dfrac{\frac{n_3}{2n_1}u_\beta(h)}{1 + z_\beta(h)/z_{\beta m}(h)} - \dfrac{\frac{n_2}{2n_1}u_\alpha(h)}{1 + z_\alpha(h)/z_{\alpha m}(h)}. \end{cases} \tag{8}$$

The harmonic ratios (HR) of the three-phase voltages on the secondary side are

$$\begin{cases} HRU_{ao}(h) = u_{ao}(h)/u_{ao}(1) \\ HRU_{bo}(h) = u_{bo}(h)/u_{bo}(1) \\ HRU_{co}(h) = u_{co}(h)/u_{co}(1) \end{cases} \tag{9}$$

In (7) and (8), the mathematical models of the three-phase harmonic voltages on the secondary side, including the load and no-load conditions, are presented. The harmonic voltages of the traction network will penetrate the low-voltage power supply system through the Scott-T transformer. The harmonic voltages of the α-phase penetrate all three-phase voltages, and the harmonic voltages of the β-phase penetrate b-phase and c-phase voltages. Obviously, when the harmonic contents of the traction network are very high, the three-phase voltage will be significantly distorted.

III. NOVEL HPF AND HARMONIC SUPPRESSION SCHEME

A. STRUCTURE AND WORKING PRINCIPLE OF THE NOVEL HPF

Since installing the HPF is one of the most feasible methods to suppress high-frequency harmonics, a novel-type HPF (NHPF) with a simple structure is proposed.

The NHPF is composed of a capacitor, a reactor and a resistor, as shown in Fig. 4. The capacitor and reactor are connected in parallel before being connected in series with the resistor.

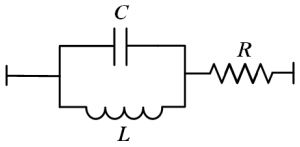

FIGURE 4. The structure of NHPF.

The impedance of the NHPF at frequency f is presented as follows:

$$z_F(f) = \frac{z_L(f) \cdot z_C(f)}{z_L(f) + z_C(f)} + z_R(f) \tag{10}$$

where z_L, z_C and z_R are the impedances of the reactor, capacitor and resistor, respectively. In addition, there are $z_F(f) = j2\pi f L_F$, $z_C(f) = 1/j2\pi f C_F$, and $z_R(f) = R_F(f)$. Here, L_F is the inductance of the reactor, C_F is the capacitance of the capacitor, and R_F is the resistance of the resistor.

Hence, (10) can be described as

$$z_F(f) = \frac{j2\pi f L_F}{1 - (2\pi f)^2 L_F C_F} + R_F(f). \tag{11}$$

As shown in Fig. 5, the impedance frequency characteristic curve can be obtained by (11).

The working principle of NHPF is discussed by the combination of (11) and Fig. 5:

(1) The capacitor and reactor have identical at impedance fundamental frequency f_N ($|z_F(f_N)| = |z_C(f_N)|$), which signifies that $1 - (2\pi f_N)^2 L_F C_F = 0$ and $z_F(f_N) \to \infty$. Under these circumstances, NHPF exhibits extremely high impedance at the fundamental frequency, so no fundamental current passes through NHPF. The amplitudes of fundamental currents of capacitor and reactor are equal, and the directions are opposite.

(2) When frequency f exceeds fundamental frequency f_N, the impedance of the NHPF rapidly diminishes with the increase in frequency f, which gradually approaches the resistance of the resistor. The NHPF exhibits very low-impedance at high frequency, and branch-C can provide a filtering high-pass path for high frequency harmonics.

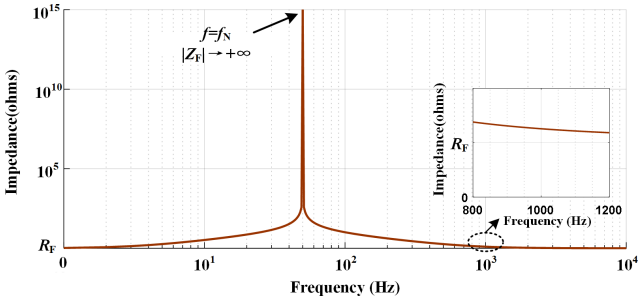

FIGURE 5. The impedance frequency characteristic curve of NHPF.

(3) When frequency f is lower than fundamental frequency f_N, the impedance of the NHPF rapidly diminishes with the decrease in frequency f, which gradually approaches the resistance of the resistor. Especially when $f = 0$ Hz, $z_F(0) = R_F(0)$. At low frequency ($f < 5$ Hz), the branch-L can provide a filtering low-pass path for low frequency harmonics.

Having almost no consumption of active power and the exchange of reactive power with the system, the NHPF does not put an additional burden on the system normal operation while filtering.

B. HARMONIC SUPPRESSION SCHEME USING NHPF

The specific harmonic suppression scheme of NHPF applied to TPSS is shown in Fig. 6.

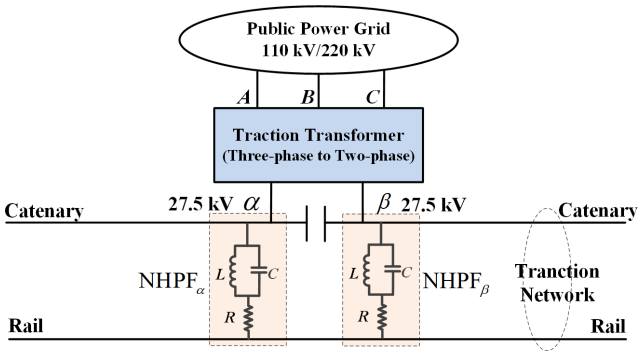

FIGURE 6. The harmonic suppression scheme of NHPF in the TPSS.

In Fig. 6, NHPF$_\alpha$ and NHPF$_\beta$ are installed in α-phase and β-phase of the TSS, respectively. Each NHPF is connected in parallel between the catenary and the rail, and high frequency harmonics are filtered through the catenary-NHPF-rail path. Although installing NHPF in the traction network can suppress high harmonics and completely solve the problems of high harmonic content and resonance, it has a high cost and intricate construction.

When the power equipment of the three-phase 380 V voltage system in the TSS is affected by high-frequency harmonics, the NHPF can be installed in the low-voltage

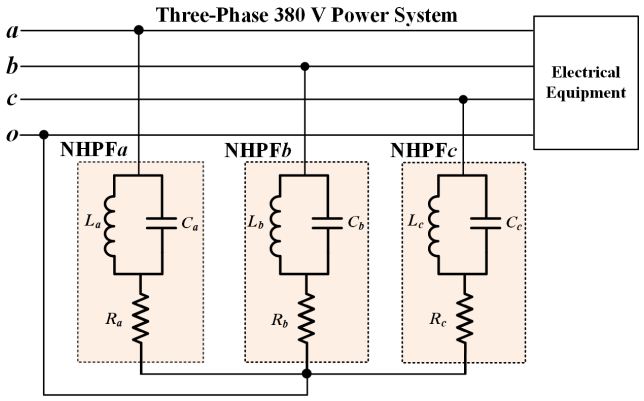

FIGURE 7. The harmonic suppression scheme of NHPF in the three-phase 380 V power system.

system first. The harmonic suppression scheme of NHPF in the three-phase 380 V power system is shown in Fig. 7.

In Fig. 7, the suppression scheme consists of three NHPFs: NHPF$_a$, NHPF$_b$ and NHPF$_c$, which are connected in parallel with the electrical equipment. The heades of NHPF$_a$, NHPF$_b$, and NHPF$_c$ are connected to line-a (a-phase), line-b (b-phase), and line-c (c-phase), respectively. Furthermore, the ends of the three NHPFs are connected to the neutral line-o.

IV. MEASUREMENT AND ANALYSIS OF HARMONICS

The Taihe TSS is located on the Beijing-Kowloon Railway Line of China. Despite the large harmonic contents of the Taihe TSS, no abnormal phenomenon has appeared on the traction network side. However, the phenomenon of equipment burnout and abnormal tripping of protection in the three-phase 380 V power system has frequently occurred. Therefore, the power quality of the Taihe TSS was measured to determine the cause of this phenomenon and propose solution. The traction transformer in the Taihe TSS is an impedance-matched balanced transformer with a rated capacity of 31.5 MVA and the phase difference of 90° between α-phase and β-phase. The main trains running on this line are HXD series of ac-dc-ac locomotives.

The step-down transformer in the Taihe TSS is a Scott-T transformer, and the parameters are shown in Table 1.

Table 1 shows that the leakage impedances of the α- phase and β-phase windings z_α and z_β are much smaller than the excitation impedances $z_{\alpha m}$ and $z_{\beta m}$. In this case, it can be considered that $z_\alpha(h) \ll z_{\alpha m}(h)$, $1 + z_\alpha(h)/z_{\alpha m}(h) \approx 1$, $z_\beta(h) \ll z_{\beta m}(h)$, $1 + z_\beta(h)/z_{\beta m}(h) \approx 1$. Therefore, (8) can be approximately equivalent to

$$\begin{cases} u_{ao}(h) = \dfrac{n_2}{n_1} u_\alpha(h) \\ u_{bo}(h) = \dfrac{n_3}{2n_1} u_\beta(h) - \dfrac{n_2}{2n_1} u_\alpha(h) \\ u_{co}(h) = -\dfrac{n_3}{2n_1} u_\beta(h) - \dfrac{n_2}{2n_1} u_\alpha(h). \end{cases} \tag{12}$$

TABLE 1. The main parameters of the Scott-T transformer.

Main element parameters	Values
Rated capacity S_N	63 kVA
Rated voltage of the primary side U_{1N}	27.5 kV
Rated current of the primary side I_{1N}	1.15 A
Percentage of short-circuit voltage U_k%	6.49
Percentage of no-load current I_0 %	2.1
Rated voltage of the secondary side U_{2N}	400 V
Rated current of the secondary side I_{2N}	90.9 A
Ratio of windings n_2/n_1	231/27500
Ratio of windings n_3/n_1	400/27500
Leakage impedance $z_{\alpha,} z_\beta$	1558.1 Ω
Excitation impedance $z_{\alpha m,} z_{\beta m}$	1138716.36 Ω

The measurement objects include α-phase bus voltage U_α, load current I_α, β-phase bus voltage U_β and load current I_β on the traction transformer secondary side, and the three-phase voltages (U_{ao}, U_{bo} and U_{co}) of the Scott-T transformer on the secondary side.

A. HARMONIC ANALYSIS OF TRACTION SIDE

Fig. 8 shows the measured waveforms of the α-phase load current I_α and β-phase load current I_β.

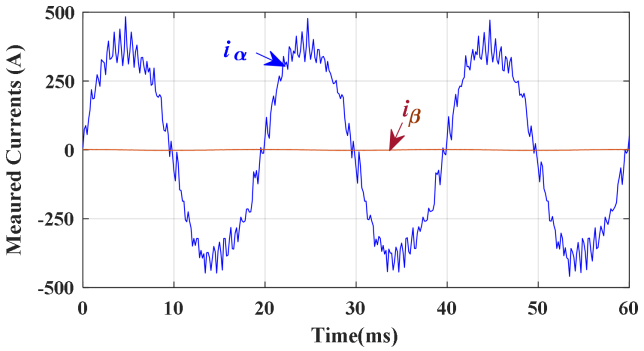

FIGURE 8. Measured waveforms of α-phase and β-phase load currents.

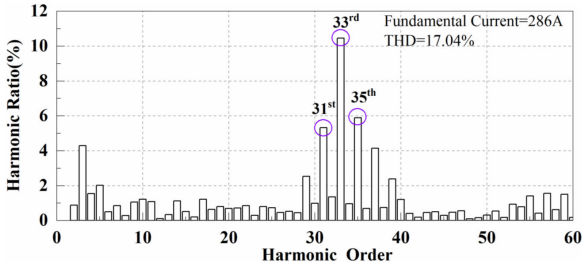

FIGURE 9. Harmonic ratios of α-phase load current.

In Fig. 8, the massive α-phase load current I_α has been significantly distorted, and the β-phase load current I_β is basically zero, which indicates that no locomotive is running on the β-phase feeder.

Through the harmonic spectrum analysis, the total harmonic distortion (THD) and each order harmonic ratio of the α-phase load current I_α are obtained, as shown in Fig. 9. The maximal THD of I_α is 17.04%, which is apparently higher than that in the normal operation of the locomotive. The main harmonics resulting in current distortion are high-frequency harmonics, especially the 31st(1550 Hz), 33rd(1650 Hz), and 35th (1750 Hz) order harmonics, with the 33rd order harmonic ratio even exceeding 10%.

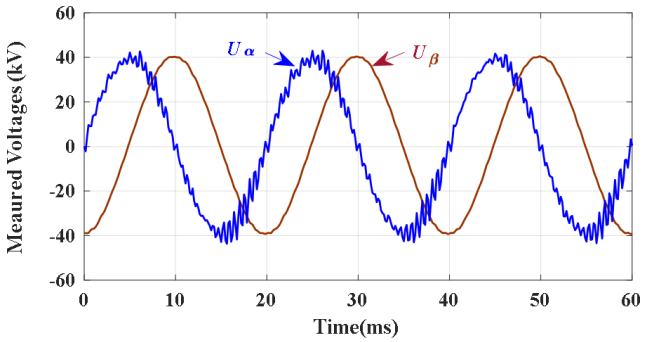

FIGURE 10. Measured waveforms of α-phase and β-phase bus voltages.

Fig. 10 shows the measured waveforms of the α-phase bus voltage U_α and β-phase bus voltage U_β. The voltage U_α has been prominently distorted by load current I_α, with extremely high-order harmonic contents. Without traction load on the β-phase line, obvious distortion is not found in voltage U_β.

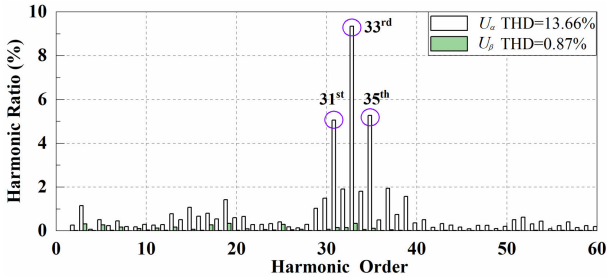

FIGURE 11. Harmonic ratios of α-phase and β-phase bus voltages.

The THD and each order harmonic ratios of U_α and U_β are shown in Fig. 11. The maximum THD of U_α is 13%, primarily due to the 31st, 33rd, and 35th order harmonics, among which the 33rd order harmonic content is the highest. In general, the distribution of harmonic ratios is identical to that of current I_α. The THD of U_β is only 0.87%, which is mainly caused by the background harmonics of the public grid side penetrating to the secondary side through the traction transformer.

B. HARMONIC ANALYSIS OF THREE-PHASE 380 V POWER SYSTEM

Fig. 12 illustrates the measured waveforms of three-phase voltages (U_{ao}, U_{bo} and U_{co}) on the secondary side of the Scott-T transformer.

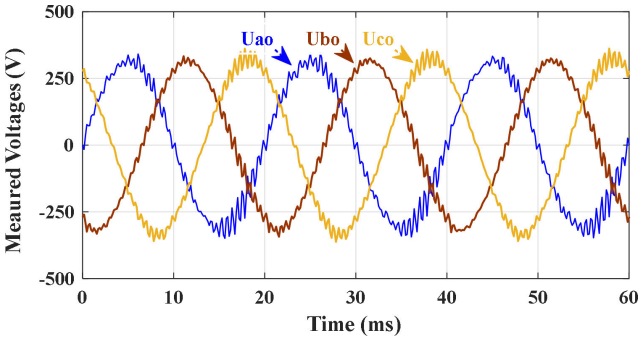

FIGURE 12. Measured waveforms of three-phase voltages.

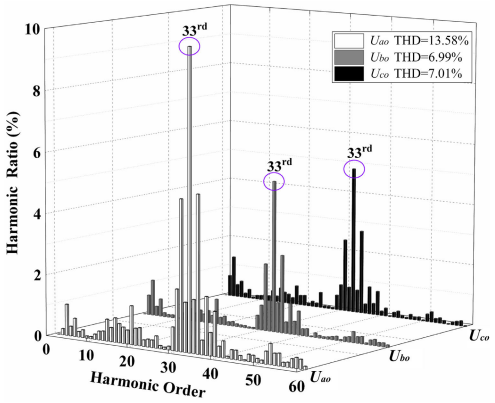

FIGURE 13. Harmonic ratios of the three-phase voltages.

In Fig. 12, all the three-phase voltages are markedly distorted, which indicates that the harmonic voltages of the α-phase on the traction side penetrate through the Scott-T transformer to the secondary side and affect all three-phase voltages.

Fig. 13 shows the harmonic spectrum analysis results of U_{ao}, U_{bo} and U_{co}. Mostly affected by α-phase harmonic voltages, the maximal THD of U_{ao} (THDU_{ao}) is 13.58%, which is notably higher than that of U_{bo} and U_{co}. (THDU_{bo} and THDU_{co}). The leading cause of three-phase voltage distortion is high-order harmonics, especially the 31st, 33rd, and 35th order harmonics, among which the 33rd order harmonic content is the highest. The distributions of harmonic ratios of the three-phase voltages are identical to U_α.

TABLE 2. The values of 31st, 33rd, and 35th order harmonic ratios (%).

Harmonic Order	U_{ao}		U_{bo}		U_{co}	
	MV	TV	MV	TV	MV	TV
31st	4.90	5.02	2.21	2.23	2.41	2.55
33rd	9.67	9.75	4.96	4.89	4.85	4.97
35th	5.12	5.27	2.56	2.53	2.77	2.73

Table 2 shows the measured values (MVs) and theoretical values (TVs) of the 31st, 33rd, and 35th order harmonic voltage ratios (%). The TVs are calculated based on (8) and (11) and the two-phase measured harmonic voltages u_α (h) and

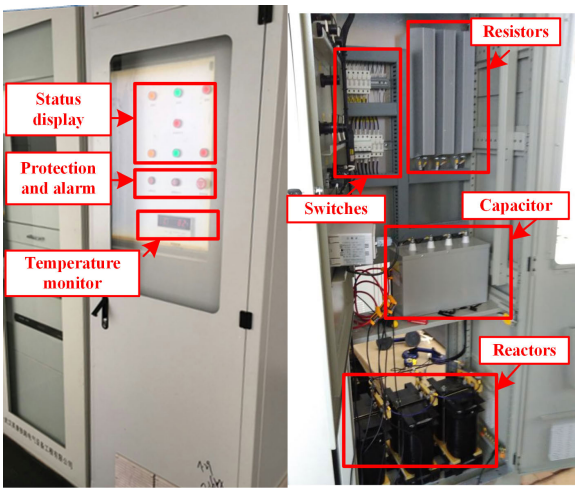

FIGURE 14. The front and internal structure of the three-phase NHPF experimental device.

$u_\beta(h)$ on the traction side. The 33rd order harmonic ratio of U_{ao} is as high as 9.67%, followed by 5.12% of the 35th order harmonic ratio and 4.9% of the 31st order harmonic ratio. Furthermore, the insignificant difference between MVs and TVs verifies the correctness of the harmonic penetration mathematical model in subsection II.B.

If U_β is also severely distorted by the traction load current, the harmonic voltages of U_β will penetrate the three-phase system side through the Scott-T transformer, which caused more serious voltage distortion. Therefore, it is necessary to install high-frequency harmonic suppression devices on the three-phase side to reduce voltage distortion.

V. EXPERIMERNTAL VERIFICATION OF THE NHPF

A. NHPF EXPERIMENTAL DEVICE

As shown in Fig. 14, a set of three-phase NHPF experimental device was designed and manufactured. Its objective is to settle the problem of excessively high-order harmonic content in low-voltage systems, and verify the feasibility and effectiveness of the harmonic suppression scheme based on NHPF in Fig. 8. The NHPF experimental device (hereafter referred to as NHPF), constituted by NHPF_a, NHPF_b, and NHPF_c, contains three resistors, a three-phase four-wire capacitor, three reactors, switches, the temperature monitor, the protection and alarm, and status display. The NHPF is placed next to the secondary equipment cabinet and connected to the three-phase voltages on the secondary side of the Scott-T transformer in the Taihe TSS.

Specific parameters of each component in the experimental device are:

(1) Reactors: $L_a = L_b = L_c = 48.3$ Mh; rated voltage 450 V; rated capacity 13.33 kW (single-phase);

(2) Resistors: $R_a = R_b = R_c = 1\ \Omega$; rated capacity 100 W;

(3) Capacitor: $C_a = C_b = C_c = 210\ \mu$F; rated voltage 450 V; rated capacity 40 kW (total capacity of the three-phase capacitor).

when designing and manufacturing the experimental device, the kind of AKMJ capacitors with good harmonic absorption capabilities is selected. According to [30], the maximum allowable total harmonic current of the selected capacitor is 25.8A, which can meet the filtering requirement.

B. HIGH-PASS CHARACTERISTIC

The measured waveforms of three-phase voltages before filtering (B.F.) and after filtering (A.F.) are shown in Fig. 15, where the NHPF is connected to the system at 32 ms.

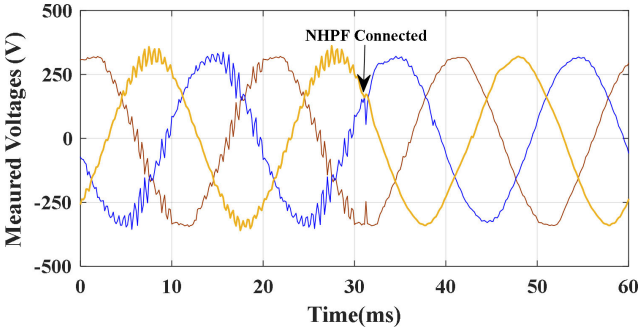

FIGURE 15. Measured waveforms of the three-phase voltages before and after filtering.

In Fig. 15, after the NHPF has been connected, the three-phase voltage waveforms are greatly enhanced, while the harmonic distortion significantly decreases.

The harmonic ratios of the three-phase voltages, i.e., U_{ao}, U_{bo} and U_{co}, before and after filtering are shown in Fig. 17. Furthermore, the THDs and typical order harmonic ratios of U_{ao}, U_{bo} and U_{co}, including 3rd, 5th, 31st, 33rd, and 35th order harmonics, are shown in Table 3.

TABLE 3. THDs and typical order harmonic ratios of the three-phase voltages before and after filtering (%).

Harmonic Order	U_{ao}		U_{bo}		U_{co}	
	B.F.	A.F.	B.F.	A.F.	B.F.	A.F.
3rd	1.40	1.42	1.51	1.58	1.29	1.31
5th	0.76	0.92	1.00	1.03	0.42	0.50
31st	2.21	0.26	1.66	0.31	2.07	0.32
33rd	8.00	0.91	5.46	0.89	5.29	0.91
35th	5.41	0.52	4.05	0.32	2.52	0.33
THD	**11.63**	**2.22**	**8.52**	**2.57**	**6.96**	**2.34**

Fig. 16 and Table 3 show that the NHPF exerts a vital effect on the suppression of high-order harmonics and has a wide filtering frequency range. After the NHPF is connected, high-order harmonic contents above the 13th order have been greatly reduced, especially those of higher orders, such as the 29th, 31st, 33rd, 35th and 37th orders. The highest 33rd order harmonic ratio of U_{ao} dropped from 8% to 0.91%, and that, of the 35th order dropped from 5.41% to 0.52%. As the NHPF can provide a low-impedance path for high-order harmonics, they can be efficaciously filtered. Notably, the high-pass characteristic has been verified.

The NHPF has no suppression effect on low-order harmonics. Due to the presence of the capacitor, low-order

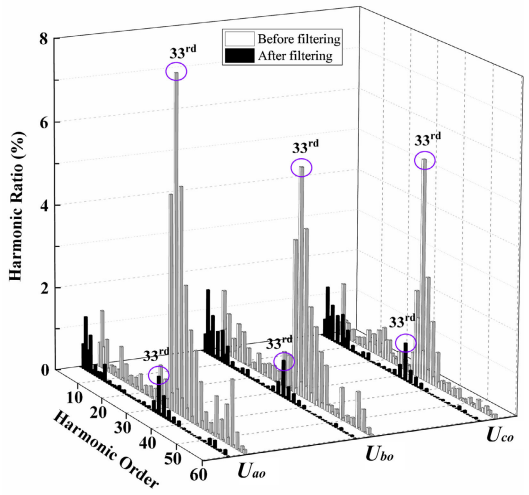

FIGURE 16. Harmonic ratios of the three-phase voltages before and after filtering.

harmonic ratios such as the 3rd and 5th orders are slightly amplified. By filtering out the higher harmonics, the total harmonic distortions of the three-phase voltages are also largely decrease. THDU_{ao}, THDU_{bo} and THDU_{co} decrease from 11.63%, 8.52%, and 6.96% before filtering to 2.22%, 2.57%, and 2.34%, respectively.

To further evaluate the harmonic suppression characteristic of the NHPF, the three-phase voltages were continuously measured for two days (48 hours). The NHPF is not connected in the first 24-hour period but the last 24-hour period. Harmonic analysis and statistics are performed on the measured three-phase voltages during the 48-hour period. In Fig. 17, there are the THDU_{ao}, THDU_{bo} and THDU_{co} in the 24-hour period before and after filtering. Moreover, the maximum values (Max. V.) and 95% probability values (95% PV) of THDU_{ao}, THDU_{bo} and THDU_{co} are shown in Table 4.

TABLE 4. Max. V and 95% PV of thd in 24-hour period.

		U_{ao}	U_{bo}	U_{co}
Max. V.	B.F.	18.98%	20.02%	15.09%
	A.F.	3.47%	4.16%	4.29%
95% PV	B.F.	7.28%	7.20%	7.19%
	A.F.	2.16%	2.62%	2.63%

Fig. 17 and Table 4 show that, the traction loads of the traction network generate a severe distortion of three-phase voltages in multiple periods of the 24-hour period before filtering, which indicates the persistence of the severe voltage distortion issue of the low-voltage three-phase system in the Taihe TSS. In the 24-hour period after the filter has been connected, the harmonic distortions of the three-phase voltages are obviously reduced and maintained in a very low range.

According to China National Standards GB/T 14549-1993, the THD limit of the phase voltage in the 380 V power system is 5%. Before filtering, the 95% probability values

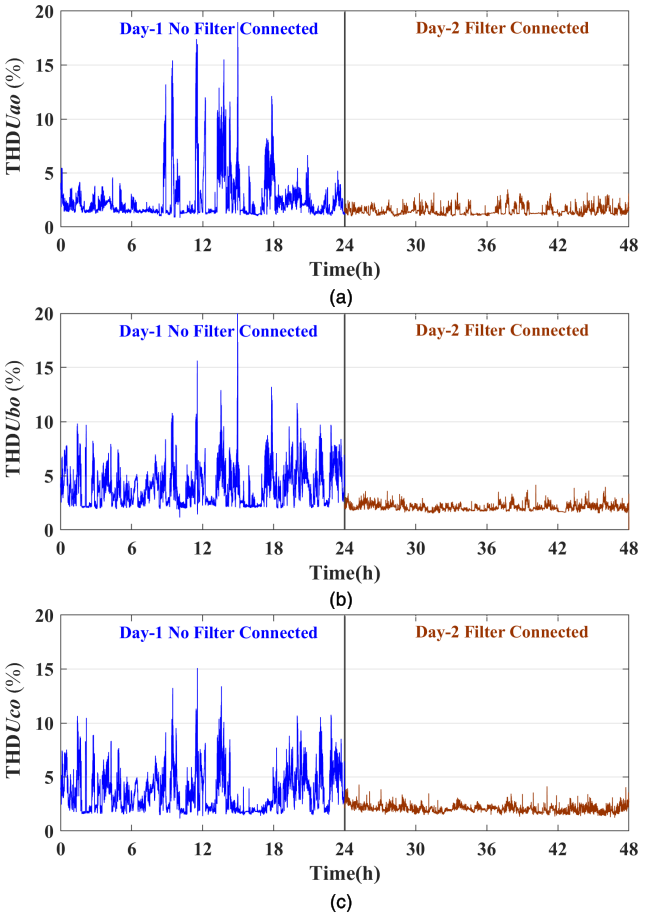

FIGURE 17. The 48h-period THD of three-phase voltages before and after the NHPF connected: (a) THDU$_{ao}$, (b) THDU$_{bo}$, (c) THDU$_{co}$.

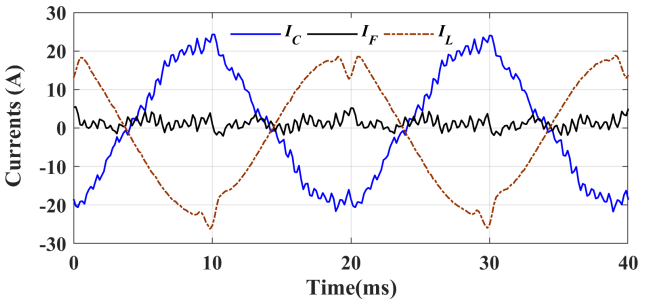

FIGURE 18. Measured current waveforms of NHPF$_a$.

of THDU_{ao}, THDU_{bo} and THDU_{co} are 7.28%, 7.20%, and 7.19%, respectively, which all exceed the limit. After filtering, the 95% probability values drop to 2.16%, 2.62%, and 2.63%, which are less than the national standard limit.

Thus, the NHPF can effectively reduce the harmonic contents of the three-phase 380 V power system under long-term operation, which prominently upgrades the power quality.

C. HIGH-IMPEDANCE CHARACTERISTIC

The filter current I_F, capacitor branch current I_C and reactor branch current I_L of the NHPF$_a$ are measured, and the measured current waveforms are shown in Fig. 18. Table 5

TABLE 5. Values of the fundamental current and harmonic currents passing through branch Ca, La and NHPFa (A).

Branch	1st	3rd	5th	31st	33rd	35th
C_a	14.59	0.634	0.532	0.206	0.773	0.447
L_a	14.45	0.587	0.484	0.020	0.029	0.016
$NHPF_a$	0.21	0.0504	0.0475	**0.223**	**0.751**	**0.438**

shows the fundamental current and main harmonic currents that pass through the branch-C_a, branch-L_a and $NHPF_a$.

Fig. 18 and Table 5 show that the filter current I_F covers components of high-order harmonics, which are mainly filtered by the capacitor branch, but no obvious high-order harmonic component appears in the reactor current I_L. Currents I_C and I_L are in opposite directions, where the fundamental currents of I_C and I_L are 14.45 A and 14.59 A, respectively. Due to manufacturing process errors and the internal resistances of the reactor, the fundamental currents of I_C and I_L are not exactly identical, but the differences are negligible. The fundamental current that flow through NHPF is 0.21 A, and the loss of $NHPF_a$ is merely 46.2 W. There are almost no fundamental losses or reactive current, and the high-impedance characteristic at the fundamental frequency is verified.

The capacitor branch contains high- and low-order harmonic currents. The reactor branch mainly contains low-order ones, while the high-order harmonic currents are very small. Under the superposition of the two branches, the currents that pass through the filter are mainly high-order harmonics, and the low-order harmonics are very small, which verifies the high-pass characteristic. Because the low-order harmonic currents occupy part of the filtering capacity of the capacitor, the filter has a smaller comprehensive filtering capacity than the capacitor.

VI. CONCLUSION

In this paper, the harmonic equivalent circuit model and the corresponding harmonic mathematical model of the Scott-T transformer, which is used as a two-phase to three-phase step-down transformer in the traction substation are established. The power quality of the TSS with high harmonic contents is measured. Theoretical analysis and measurement results show that the high-frequency harmonics of the traction network can be considered the background harmonics that penetrate into the secondary side of the Scott-T transformer, which causes serious three-phase voltage distortion of the TSS, and the degree of distortion and harmonic distribution are identical to as those of the traction network. The total harmonic distortion of the three-phase voltage in the measured TSS seriously exceeds the limit, which endangers the operational safety of the electrical equipment. To solve this problem, a three-phase high-frequency suppression scheme based on the NHPF is proposed, and an experimental device is developed. The harmonic analysis results before and after filtering show that the NHPF can effectively filter high-frequency harmonics and has a wide filtering frequency range, which can greatly reduce the voltage distortion of the three-phase system. Meanwhile, the NHPF is featured with extremely low loss, has the characteristics of high-pass at high frequencies and high-impedance at the fundamental frequency, and does not exchange reactive power with the power supply system at the fundamental frequency. The effectiveness and feasibility of the suppression scheme based on NHPF have been verified.

REFERENCES

[1] J. Holtz and H.-J. Kelein, "The propagation of harmonic currents generated by inverter-fed locomotives in the distributed overhead supply system," *IEEE Trans. Power Electron.*, vol. 4, no. 2, pp. 169–174, Apr. 1989.
[2] L. He, J. Xiong, H. Ouyang, P. Zhang, and K. Zhang, "High-performance indirect current control scheme for railway traction four-quadrant converters," *IEEE Trans. Ind. Electron.*, vol. 61, no. 12, pp. 6645–6654, Dec. 2014.
[3] S. V. Raygani, A. Tahavorgar, S. S. Fazel, and B. Moaveni, "Load flow analysis and future development study for an AC electric railway," *IET Elect. Syst. Transp.*, vol. 2, no. 3, pp. 139–147, Sep. 2012.
[4] G. W. Chang, H.-W. Lin, and S.-K. Chen, "Modeling characteristics of harmonic currents generated by high-speed railway traction drive converters," *IEEE Trans. Power Del.*, vol. 19, no. 2, pp. 766–773, Apr. 2004.
[5] S. Leva, "Dynamic stability of isolated system in the presence of PQ disturbances," *IEEE Trans. Power Del.*, vol. 23, no. 2, pp. 831–840, Apr. 2008.
[6] E. Mollerstedt and B. Bernhardsson, "Out of control because of harmonics-an analysis of the harmonic response of an inverter locomotive," *IEEE Control Syst. Mag.*, vol. 20, no. 4, pp. 70–81, Aug. 2000.
[7] L. Guo, Q. Li, and Y. Xu, "Study on harmonic resonance of traction line in electrified high-speed traction system," in *Proc. Int. Conf. Sustain. Power Gener. Supply*, Nanjing, China, Apr. 2009, pp. 1–4.
[8] M. Brenna, A. Capasso, M. C. Falvo, F. Foiadelli, R. Lamedica, and D. Zaninelli, "Investigation of resonance phenomena in high speed railway supply systems: Theoretical and experimental analysis," *Electr. Power Syst. Res.*, vol. 81, no. 10, pp. 1915–1923, Oct. 2011.
[9] H. Lee, C. Lee, G. Jang, and S. Kwon, "Harmonic analysis of the Korean high-speed railway using the eight-port representation model," *IEEE Trans. Power Del.*, vol. 21, no. 2, pp. 979–986, Apr. 2006.
[10] J. Holtz and J. O. Krah, "On-line identification of the resonance conditions in the overhead supply line of electric railways," *Archiv für Elektrotechnik*, vol. 74, no. 1, pp. 99–106, Jan. 1990.
[11] H. Hu, P. Pan, Y. Song, and Z. He, "A novel controlled frequency band impedance measurement approach for single-phase railway traction power system," *IEEE Trans. Ind. Electron.*, vol. 67, no. 1, pp. 244–253, Jan. 2020, doi: 10.1109/TIE.2019.2896297.
[12] R. Cella, G. Giangaspero, A. Mariscotti, A. Montepagano, P. Pozzobon, M. Ruscelli, and M. Vanti, "Measurement of AT electric railway system currents at power-supply frequency and validation of a multiconductor transmission-line model," *IEEE Trans. Power Del.*, vol. 21, no. 3, pp. 1721–1726, Jul. 2006.
[13] A. Dolara, M. Gualdoni, and S. Leva, "Impact of high-voltage primary supply lines in the 2 × 25 kV–50 Hz railway system on the equivalent impedance at pantograph terminals," *IEEE Trans. Power Del.*, vol. 27, no. 1, pp. 164–175, Jan. 2012.
[14] Z. He, H. Hu, Y. Zhang, and S. Gao, "Harmonic resonance assessment to traction power-supply system considering train model in China high-speed railway," *IEEE Trans. Power Del.*, vol. 29, no. 4, pp. 1735–1743, Aug. 2014.
[15] H. Hu, Z. He, Y. Zhang, and S. Gao, "Modal frequency sensitivity analysis and application using complex nodal matrix," *IEEE Trans. Power Del.*, vol. 29, no. 2, pp. 969–971, Apr. 2014.
[16] X. Lv, X. Wang, Y. Che, and R. Fu, "Eigenvalue-based harmonic instability analysis of electrical railway vehicle-network system," *IEEE Trans. Transport. Electrific.*, vol. 5, no. 3, pp. 727–744, Sep. 2019.
[17] W. Song, S. Jiao, Y. W. Li, J. Wang, and J. Huang, "High-frequency harmonic resonance suppression in high-speed railway through single-phase traction converter with LCL filter," *IEEE Trans. Transport. Electrific.*, vol. 2, no. 3, pp. 347–356, Sep. 2016.
[18] H. Cui, W. Song, X. Feng, and X. Ge, "High-frequency resonance suppression of high-speed railways in China," *IET Electr. Syst. Transp.*, vol. 6, no. 2, pp. 88–95, Jun. 2016.

[19] K. Song, G. Konstantinou, W. Mingli, P. Acuna, R. P. Aguilera, and V. G. Agelidis, "Windowed SHE-PWM of interleaved four-quadrant converters for resonance suppression in traction power supply systems," *IEEE Trans. Power Electron.*, vol. 32, no. 10, pp. 7870–7881, Oct. 2017.
[20] X. Zhang, J. Chen, G. Zhang, R. Qiu, and Z. Liu, "The WRHE-PWM strategy with minimized THD to suppress high-frequency resonance instability in railway traction power supply system," *IEEE Access*, vol. 7, pp. 104478–104488, 2019.
[21] S. Liu, F. Lin, X. Fang, Z. Yang, and Z. Zhang, "Train impedance reshaping method for suppressing harmonic resonance caused by various harmonic sources in trains-network systems with auxiliary converter of electrical locomotive," *IEEE Access*, vol. 7, pp. 179552–179563, 2019.
[22] K. Song, W. Mingli, S. Yang, Q. Liu, V. G. Agelidis, and G. Konstantinou, "High-order harmonic resonances in traction power supplies: A review based on railway operational data, measurements, and experience," *IEEE Trans. Power Electron.*, vol. 35, no. 3, pp. 2501–2518, Mar. 2020.
[23] H. Hu, Z. He, and S. Gao, "Passive filter design for China high-speed railway with considering harmonic resonance and characteristic harmonics," *IEEE Trans. Power Del.*, vol. 30, no. 1, pp. 505–514, Feb. 2015.
[24] J. Wang, M. Zhang, S. Li, T. Zhou, and H. Du, "Passive filter design with considering characteristic harmonics and harmonic resonance of electrified railway," in *Proc. 8th Int. Conf. Mech. Intell. Manuf. Technol. (ICMIMT)*, Cape Town, South Africa, Feb. 2017, pp. 174–178.
[25] O. F. Kececioglu, H. Acikgoz, and M. Sekkeli, "Advanced configuration of hybrid passive filter for reactive power and harmonic compensation," *SpringerPlus*, vol. 5, no. 1, p. 1228, Dec. 2016.
[26] O. F. Kececioglu, H. Acikgoz, C. Yildiz, A. Gani, and M. Sekkeli, "Power quality improvement using hybrid passive filter configuration for wind energy systems," *J. Electr. Eng. Technol.*, vol. 12, no. 1, pp. 207–216, Jan. 2017.
[27] Y. Zhao, Q. Li, and F. Zhou, "Resonance suppression based on wave-trap high-pass filter for high-speed railway," (in Chinese), *Electr. Power Autom. Equip.*, vol. 35, no. 4, pp. 139–144, Apr. 2015.
[28] B. Luo, S. Xie, J. Sun, and M. Chen, "Harmonic resonance suppression based on wave-trap high-pass filter," in *Proc. 14th IEEE Conf. Ind. Electron. Appl. (ICIEA)*, Xi'an, China, Jun. 2019, pp. 1274–1279.
[29] Y. Li and P. A. Crossley, "Voltage balancing in low-voltage radial feeders using Scott transformers," *IET Gener., Transmiss. Distrib.*, vol. 8, no. 8, pp. 1489–1498, Aug. 2014.
[30] C. Haozhong, L. Peihong, C. Zhangchao, S. Hiroshi, and Y. Naoto, "Optimal selection of parameteric power filters," *Power Syst. Technol.*, vol. 19, no. 10, pp. 42–48, Oct. 1995.

YUANZHE ZHAO (Member, IEEE) received the B.S. degree in electrical engineering and automation and the Ph.D. degree in power systems and automation from Southwest Jiaotong University, Chengdu, China, in 2009 and 2016, respectively.

He holds a postdoctoral position at the College of Transportation Engineering and the National Maglev Transportation Engineering Technology Research and Development Center, Tongji University, Shanghai, China. His research interests include power quality analysis and control, harmonic analysis, and the control of electrical drives.

LINJIE REN (Graduate Student Member, IEEE) received the B.S. degree in industrial automation and the M.S. degree in control theory and control engineering from Lanzhou Jiaotong University, Lanzhou, China, in 2011 and 2017, respectively. He is currently pursuing the Ph.D. degree with Tongji University. His current research interests include control with applications to mechatronics systems, and power quality analysis and control.

GUOBIN LIN received the B.S. degree in electric machine from Zhejiang University, Hangzhou, China, in 1986, and the M.S. degree in electrical engineering from Southwest Jiaotong University, Chengdu, China, in 1989.

He is currently a Professor and the Deputy Director of the National Maglev Transportation Engineering Technology Research and Development Center, Tongji University, Shanghai, China. His research interests include maglev vehicles and linear drive research.

Mr. Lin has been a member of the Steering Committee of International Maglev System and the Linear Drive Conference since 2014.

FEI PENG (Member, IEEE) received the B.S. degree in electronics engineering and automation and the Ph.D. degree in power systems and automation from Southwest Jiaotong University, Chengdu, China, in 2009 and 2014, respectively.

He is currently working with the College of Electrical Engineering, Qingdao University, Qingdao, China. His research interest includes the levitation control technology of maglev train.